



Article

# Analysis of the Electron Density of a Water Molecule Encapsulated by Two Cholic Acid Residues

María Pilar Vázquez-Tato <sup>1</sup>, Julio A. Seijas <sup>1,\*</sup>, Francisco Mejjide <sup>2</sup>, Santiago de Frutos <sup>2</sup> and José Vázquez Tato <sup>2</sup>

<sup>1</sup> Departamento de Química Orgánica, Facultade de Ciencias, Universidade de Santiago de Compostela, Campus Terra, 27080 Lugo, Spain

<sup>2</sup> Departamento de Química Física, Facultade de Ciencias, Universidade de Santiago de Compostela, Campus Terra, 27080 Lugo, Spain

\* Correspondence: julioa.seijas@usc.es

**Abstract:** Cholic acid is a trihydroxy bile acid with a nice peculiarity: the average distance between the oxygen atoms (O7 and O12) of the hydroxy groups located at C7 and C12 carbon atoms is 4.5 Å, a value which perfectly matches with the O/O tetrahedral edge distance in Ih ice. In the solid phase, they are involved in the formation of hydrogen bonds with other cholic acid units and solvents. This fact was satisfactorily used for designing a cholic dimer which encapsulates one single water molecule between two cholic residues, its oxygen atom (Ow) being exactly located at the centroid of a distorted tetrahedron formed by the four steroid hydroxy groups. The water molecule participates in four hydrogen bonds, with the water simultaneously being an acceptor from the 2 O12 (hydrogen lengths are 2.177 Å and 2.114 Å) and a donor towards the 2 O7 (hydrogen bond lengths are 1.866 Å and 1.920 Å). These facts suggest that this system can be a nice model for the theoretical study of the formation of ice-like structures. These are frequently proposed to describe the water structure found in a plethora of systems (water interfaces, metal complexes, solubilized hydrophobic species, proteins, and confined carbon nanotubes). The above tetrahedral structure is proposed as a reference model for those systems, and the results obtained from the application of the atoms in molecules theory are presented here. Furthermore, the structure of the whole system allows a division into two interesting subsystems in which water is the acceptor of one hydrogen bond and the donor of another. The analysis of the calculated electron density is performed through its gradient vector and the Laplacian. The calculation of the complexation energy used correction of the basis set superposition error (BSSE) with the counterpoise method. As expected, four critical points located in the H...O bond paths were identified. All calculated parameters obey the proposed criteria for hydrogen bonds. The total energy for the interaction in the tetrahedral structure is 54.29 kJ/mol, while the summation obtained of the two independent subsystems and the one between the alkyl rings without water is only 2.5 kJ/mol higher. This concordance, together with the calculated values for the electron density, the Laplacian of the electron density, and the lengths of the oxygen atom and the hydrogen atom (involved in the formation of each hydrogen bond) to the hydrogen bond critical point, suggests that each pair of hydrogen bonds can be considered independent of each other.

**Keywords:** bile acid; cholic acid; hydrogen bond; atoms in molecules theory; electronic density; critical points



**Citation:** Vázquez-Tato, M.P.; Seijas, J.A.; Mejjide, F.; de Frutos, S.; Vázquez Tato, J. Analysis of the Electron Density of a Water Molecule Encapsulated by Two Cholic Acid Residues. *Int. J. Mol. Sci.* **2023**, *24*, 5359. <https://doi.org/10.3390/ijms24065359>

Academic Editor: Mihai V. Putz

Received: 7 February 2023

Revised: 28 February 2023

Accepted: 8 March 2023

Published: 10 March 2023



**Copyright:** © 2023 by the authors. Licensee MDPI, Basel, Switzerland. This article is an open access article distributed under the terms and conditions of the Creative Commons Attribution (CC BY) license (<https://creativecommons.org/licenses/by/4.0/>).

## 1. Introduction

During evolution, nature has learned to distinguish what works from what does not. Consequently, all living beings have adopted successful mechanisms and molecules for solving the challenges they must face to achieve a particular purpose. The knowledge of the involved processes provides the scientific community with strategies for designing new molecules with specific properties to reach a desired target. According to Menger [1], the design of a molecule from the beginning with a list of optimal functionalities is not an

easy task, although it may be facilitated by emulating the biological mechanisms. Among many other molecules, bile acids fulfill the steps described by Lenh [2] involved in the evolution of matter. Hofmann [3] has discussed their structural variation and its possible evolutionary significance. The steroid nucleus has been implied in a key evolutionary step as it is ubiquitous in animals (as hormones, cholesterol, and bile acids) and plants (as brassinosteroids).

All the above information led us to use natural bile acids as raw materials for synthesizing derivatives that self-organize into new supramolecular structures [4–7]. Among the designs, we studied a cholic dimer, which encapsulates one single water molecule between two cholic residues [8].

Bile acids (BAs) have a bifacial polarity since the hydroxy groups (up to three at C3, C7, and C12 carbon atoms) lie beneath the plane of the steroid nucleus (hydrophilic  $\alpha$ -side). The characterization of the crystal structures of BA and their derivatives by X-ray analysis has been a topic of interest for years [9–17]. Common to all crystal structures is that the hydroxy groups are always involved in the formation of hydrogen bonds (HB) with other BA molecules, the solvent, or both species. In cholic acid (Figure 1), the average hydrogen bond distances formed by the C7-OH and C12-OH hydroxy groups (from here these oxygen atoms will be identified as O<sup>7</sup> and O<sup>12</sup>) with water have been recompiled with values of  $2.79 \pm 0.09 \text{ \AA}$  and  $2.86 \pm 0.10 \text{ \AA}$ , respectively [9], the O<sup>7</sup>/O<sup>12</sup> distance being  $4.5 \text{ \AA}$ , a value which perfectly matches with the O/O tetrahedral edge distance in I<sub>h</sub> ice, respectively [18,19]. These facts suggest the design of the cholic dimer mentioned previously [8]. In this complex, the water oxygen atom (O<sup>w</sup>) is exactly located at the centroid of a distorted tetrahedron formed by the four steroid hydroxy groups (Figure 2, left). Both O<sup>12</sup>-H are hydrogen bond donors towards O<sup>w</sup>, while both O<sup>7</sup>-H are acceptors from O<sup>w</sup>. Figure 2 (right) shows the values for the four hydrogen bonds. It may be noticed that the O<sup>7</sup>⋯O<sup>w</sup> distances are close to the one measured in I<sub>h</sub> ice while the O<sup>12</sup>⋯O<sup>w</sup> distances match the O⋯O distance observed in the water dimer in gas phase (see below). In his review on the hydrogen bond in the solid state, Steiner [20] has indicated average values of  $1.880(2) \text{ \AA}$  and  $2.825(2) \text{ \AA}$  for H⋯OH<sub>2</sub> and O⋯O distances, respectively, for the dimer HO-H⋯OH<sub>2</sub>.

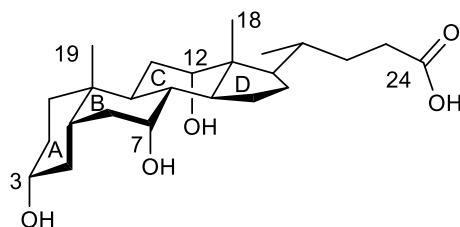


**Figure 1.** Structure of cholic acid. Significant carbon atoms are numbered as well as the four rings of the steroid nucleus. In the text, the numbers of oxygen atoms are those of the carbon atoms to which they are bonded.

The term ice-like is frequently used to describe the structure of water found in a plethora of systems. Among them, we can mention water clusters (H<sub>2</sub>O)<sub>n</sub> in compounds as metal-organic networks in the solid state [21], liquid water solubilizing hydrophobic species [22–25] or proteins [26,27], and in water interfaces [28]. However, Bonn et al. [29] have concluded that the vibrational spectrum of water at both water-lipid and water-protein interfaces is inconsistent with the presence of “ice-like” structures. Ice-like behavior is also recognized in carbon nanotubes (CNTs) [30–33] and in sub-nanometer carbon slit pores [34], but it can be suppressed in supercooled water in tight confinements [35].

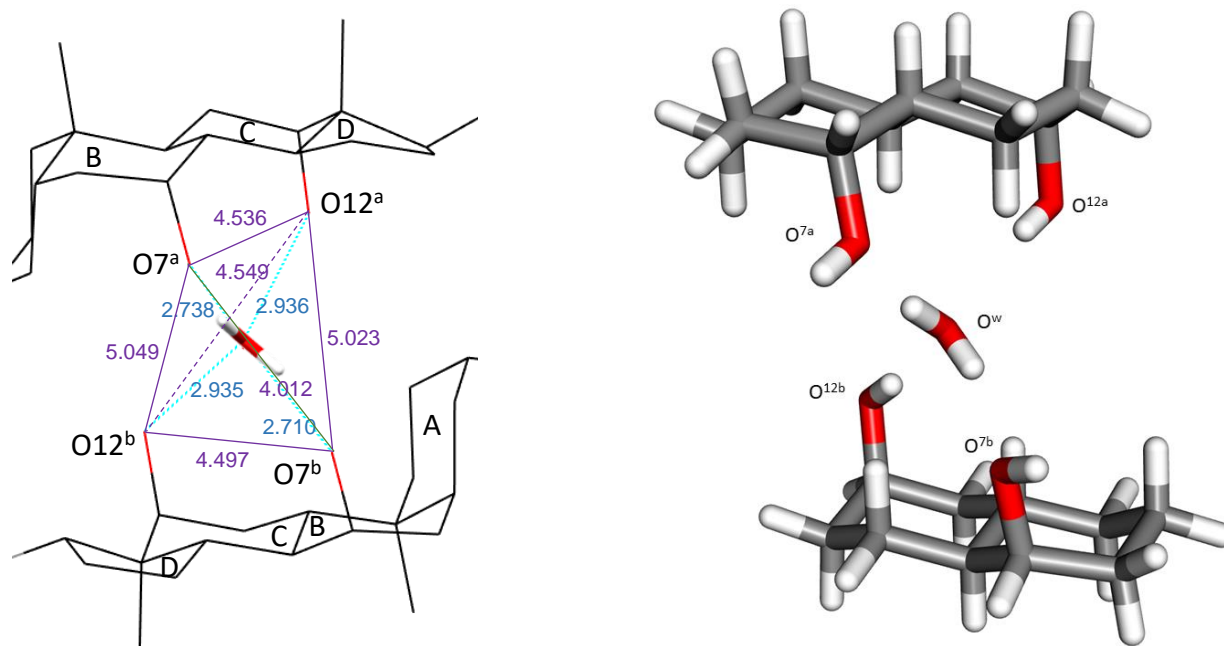


**Figure 2.** **Left:** Oxygen–Oxygen distances (lines and data in amethyst color) of the tetrahedron formed by the  $O^7$ -H and  $O^{12}$ -H hydroxy atoms of the two steroid residues encapsulating a water molecule located at their centroid [8]. The four hydrogen bonds are indicated with blue lines, as are the hydrogen bond distance values ( $O^w$ -H $\cdots$   $O^7$  and  $O^{12}$ -H $\cdots$   $O^w$ ). All data in Å. **Right:** Simplified system model.

Weissmann et al. [36] self-limited their study on the hydrogen bond in an ice-like structure to “the interactions of one water molecule with its four nearest neighbors” somehow accepting that a water molecule should form four hydrogen bonds, the oxygen atom simultaneously being a hydrogen bond donor and acceptor (two of each). Therefore, in the analysis of published structures that we have carried out, only tetrahedral water and the interaction with neutral oxygen atoms have been considered. Different  $O\cdots O$  hydrogen bond distances are observed in water clusters in metal-organic complexes, depending on the role of the oxygen atom as acceptor or donor of a hydrogen bond [21,37,38]. This difference can be as high as 0.17 Å (measured from cif files) [38]. In our opinion, this distinction has not been sufficiently analyzed in the literature. Obviously, such a distinction cannot be made in  $I_h$  ice, as all  $O\cdots O$  hydrogen bond distances have the same value.

All the previous facts, together with the perfect distinction between hydrogen bond donors and acceptors for water linked to a tetrahedral hydroxy structure, surrounded by apolar alkyl skeletons, constitute a unique model to pursue a theoretical study. Keeping this in mind, the “atoms in molecules” (AIM) theory [39,40] has been applied to a model system derived from this ice-like structure. On the other hand, when analyzing BA crystals for the acceptance of the formation of a hydrogen bond, the geometric criteria (bond lengths and angles) [41] have been used exclusively. This is the first time that the AIM theory has been applied to a BA crystal.

## 2. Results and Discussion

### 2.1. Complex $O^{12a}$ -H $\cdots$ $O^w$ -H $\cdots$ $O^{7a}$ // $O^{12b}$ -H $\cdots$ $O^w$ -H $\cdots$ $O^{7b}$

The electron density,  $\rho$ , is the starting point of the AIM theory. Its topology is easily deduced from the gradient vector,  $\nabla\rho$ , and the Laplacian,  $\nabla^2\rho$ . The electron density is usually visualized by drawing contour lines connecting electron density points with the same value. Figures 3 and 4 show two examples for the present system. In Figure 3, the plane is defined by the oxygen nuclei  $O^{7a}$ ,  $O^{7b}$ , and  $O^w$ , while in Figure 4, the plane is defined by

oxygen atoms  $O^{12a}$ ,  $O^{12b}$ , and  $O^w$ . The thin gray lines are defined by infinitesimal gradient vectors, which describe gradient paths.

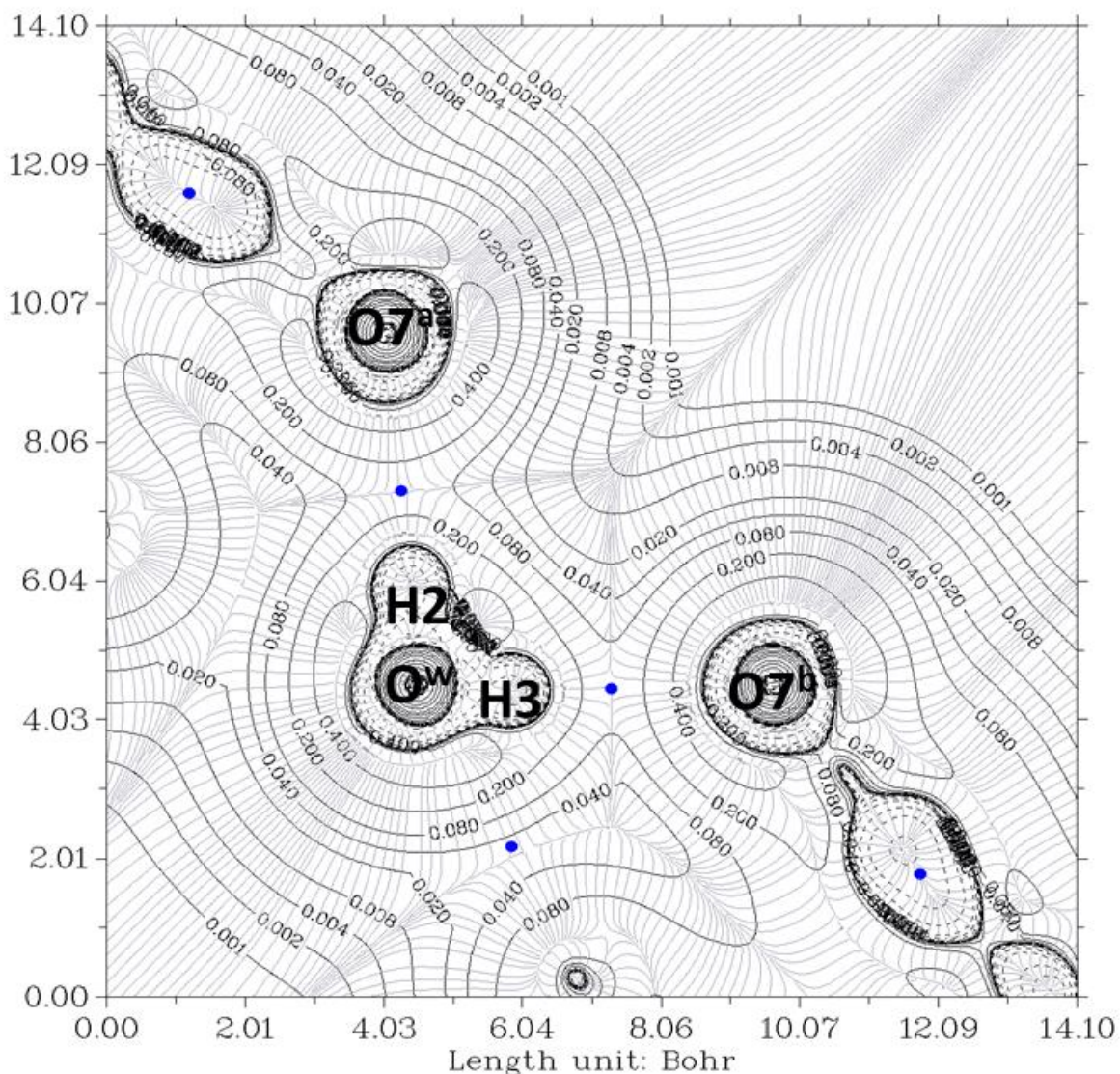


**Figure 3.** The electron density contour of the  $O^{12a}\text{-H}\cdots O^w\text{-H}\cdots O^{7a}$ // $O^{12b}\text{-H}\cdots O^w\text{-H}\cdots O^{7b}$  complex (thin black lines) and BCP (3,-1) (blue dots). The plane is defined by  $O^{7a}$ ,  $O^{7b}$ , and  $O^w$  oxygen atoms of the pseudo-bile acid residues and water, respectively. Thin gray lines correspond to the gradient of the electron density.

When  $\nabla^2\rho < 0$ , the electronic charge is locally concentrated, as in the case of covalent bonds [42]. When  $\nabla^2\rho > 0$ , the electronic charge is locally depleted [40], resulting in what are called *closed-shell* interactions. This happens in hydrogen bonds (HB), in which the charge concentrations are separately localized in the basins of the neighboring atoms [43]. Figure 5 shows bond critical points where the gradient  $\nabla\rho$  vanishes. Numbers 17, 43, 50, and 59, located between hydrogen and oxygen atoms, correspond to hydrogen bond critical points (HBCP), which are (3,-1) saddle points. Other numbers correspond to covalent bonds (located, for instance, between two carbon atoms).

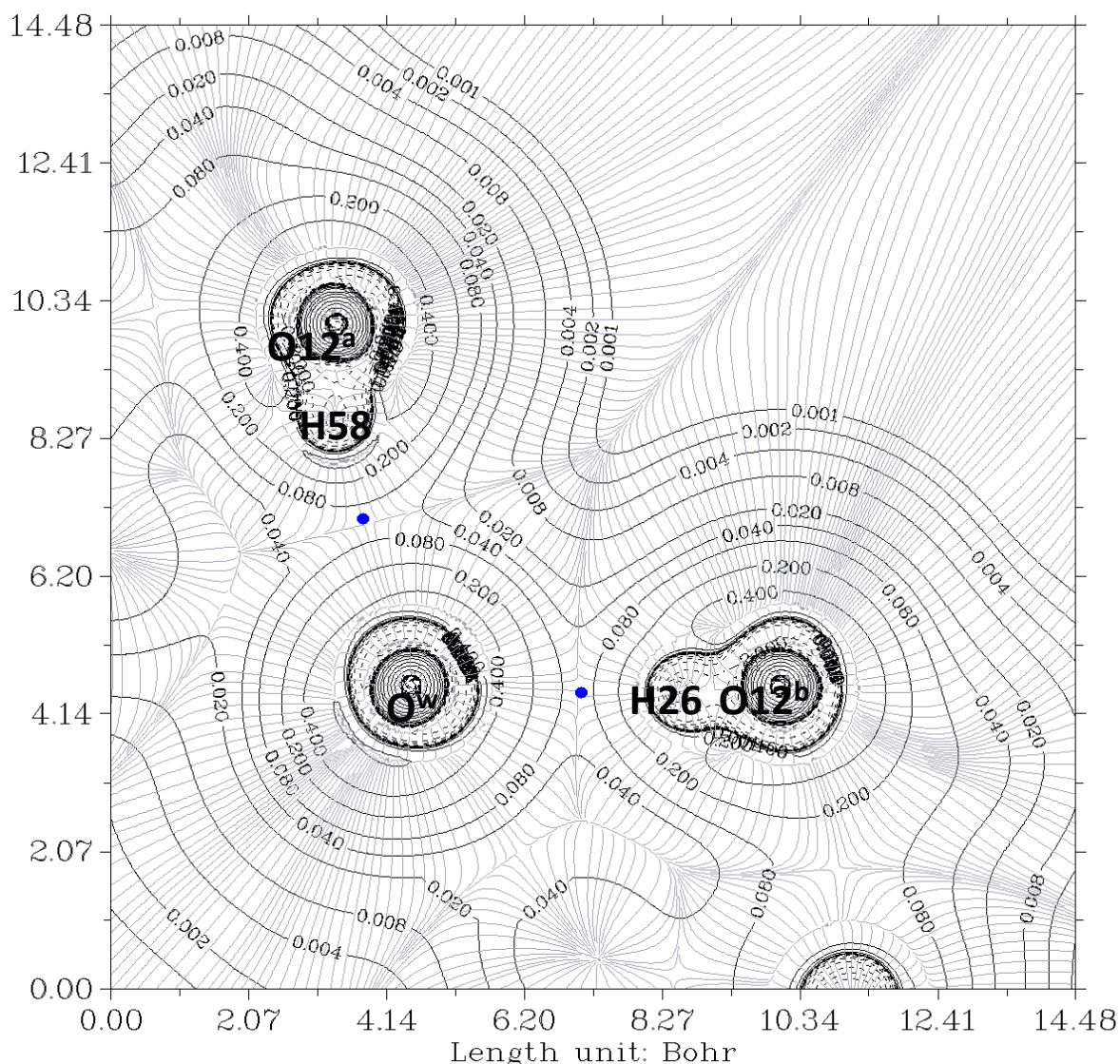


**Figure 4.** The electron density contour of the  $O^{12a}\text{-H}\cdots O^w\text{-H}\cdots O^{7a}/O^{12b}\text{-H}\cdots O^w\text{-H}\cdots O^{7b}$  complex (thin black lines) and BCP (3,-1) (blue dots). The plane is defined by the  $O^{12a}$ ,  $O^{12b}$ , and  $O^w$  oxygen atoms of the bile acid residues and water, respectively. Thin gray lines correspond to the gradient of the electron density.

In Figure 3, the contour lines of the electronic density around the water oxygen ( $O^w$ ) basin resemble a Mickey Mouse profile. This is a consequence of the fact that the two hydrogen atoms of water (named H2 and H3 in the Figure) form covalent bonds with  $O^w$ . In other words,  $O^w$  is behaving as a HB donor, while from this perspective, the basin of the  $O^7$  oxygen atom has a circle shape. Similarly, Figure 4 shows the contour lines of the hydrogen bonds between  $O^w$  and the two  $O^{12}\text{-H}$  hydroxy groups. The plane in the Figure is defined by these three oxygen atoms. Now the contour around the  $O^w$  resembles a basin, while the profiles around the  $O^{12}\text{-H}$  groups resemble peanuts. The two  $O^{12}$  are donors, and  $O^w$  is the acceptor. Furthermore, the bond paths of the four hydrogen bonds link the expected two atoms, the hydrogen and the acceptor. It is evident that the first condition of the criteria to characterize a hydrogen bond published by Popelier [42,44] is fulfilled. Furthermore, according to Popelier [42], the  $\rho$  values at the HBCP,  $\rho_b$ , should be in the range 0.002–0.035 au, Table 1 showing that this is the case for the four HB. These values are about one order of magnitude smaller than those found for a covalent bond ( $\rho_b = 0.391$  au,

for O-H in H<sub>2</sub>O) [45]. On the other hand, it may be noticed that the values when water is a donor (towards O<sup>7</sup>) are almost double than when it behaves as an acceptor (from O<sup>12</sup>).

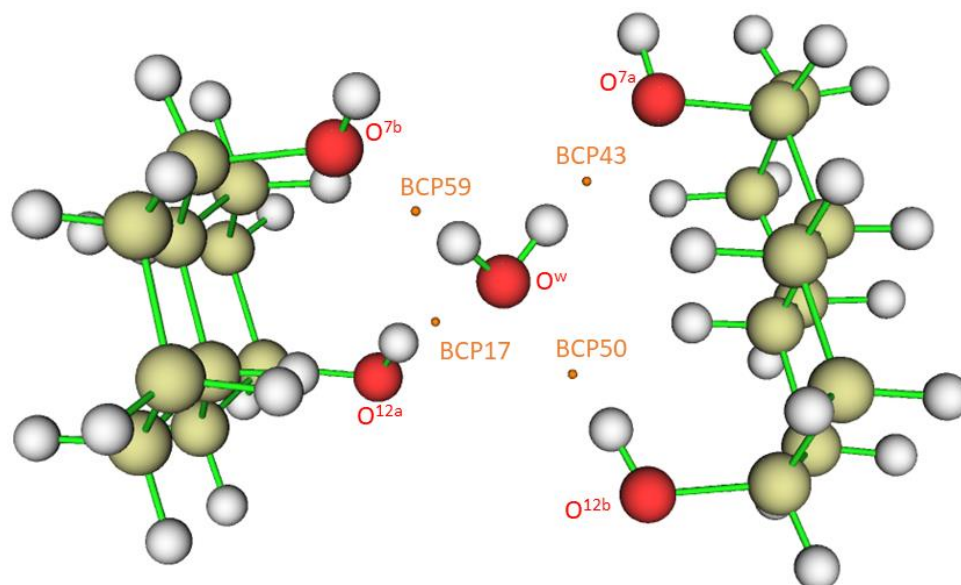


**Figure 5.** Bond critical points (BCP) and hydrogen bond critical points (HBCP) obtained for the complex O<sup>12a</sup>-H...O<sup>w</sup>-H...O<sup>7a</sup>//O<sup>12b</sup>-H...O<sup>w</sup>-H...O<sup>7b</sup>. HBCPs are identified with numbers 17, 43, 50, and 59.

The correlation between the O-O length and  $\rho_b$  has been published [46,47]. The shorter the former, the higher the latter. The values obtained here differ by less than  $\pm 0.004$  au with those obtained from the equation  $\rho_b = 2.71 \times \exp(-2.40 \times r_{O...H})$ , ( $r_{O...H}$  in Å) [47]. They also match values recompiled by Steiner [20] (see Figure 3 of this reference).

**Table 1.** Lengths involved in the formation of hydrogen bonds were determined from the crystal structure and calculated along with electron density and Laplacian values.

Complex O <sup>12a</sup> -H...O <sup>w</sup> -H...O <sup>7a</sup> //O <sup>12b</sup> -H...O <sup>w</sup> -H...O <sup>7b</sup>				
Identification HBCP (Figure 5)	50	59	17	43
Property at HBCP	O <sup>12a</sup> -H...O <sup>w</sup>	O <sup>w</sup> -H...O <sup>7a</sup>	O <sup>12b</sup> -H...O <sup>w</sup>	O <sup>w</sup> -H...O <sup>7b</sup>
O-O length/Å crystal	2.936	2.738	2.935	2.710
O...H length/Å crystal	2.114	1.920	2.177	1.866
Electron density $\rho_b$ , au	0.0154	0.0239	0.0138	0.0270
$\rho_b$ calculated according to [47]	0.0170	0.0270	0.0146	0.0308
Laplacian of the electron density at HBCP, $\nabla^2\rho_b$ , au	0.0667	0.106	0.0616	0.118
HBCP...O length/Å, $r_1$	1.355	1.242	1.383	1.217
HBCP...H length/Å, $r_2$	0.759	0.679	0.795	0.650
$r_1 + r_2 = r_{O...H}$ length/Å	2.114	1.921	2.178	1.867
$\Delta r_O = r_{vdW}^O - r_1/\text{Å}$	0.225	0.338	0.197	0.363
$\Delta r_H = r_{vdW}^H - r_2/\text{Å}$	0.341	0.421	0.305	0.450

A third criterion proposed by Popelier refers to the Laplacian of the charge density evaluated at the bond critical point, where charge density is a local minimum along the bond path, i.e.,  $\rho_b$  is locally depleted with respect to neighboring points along the bond

path. The range values (Table 1) are also within the proposed range of 0.024–0.139 au.  $\nabla^2\rho_b$  follows an analogous dependence with the O–O length than  $\rho_b$ .

Previous  $\rho_b$  and  $\nabla^2\rho_b$  values may be compared with those for the water dimer, H–O–H  $\cdots$  OH<sub>2</sub> in the gas phase. The water dimer is a system of two water molecules bound by a single hydrogen bond, often used as the paradigmatic system [48,49]. Its equilibrium geometry is well-known, as is the dissociation energy. The dimer has a “trans-linear” structure, and the O  $\cdots$  O distance was first measured by Dyke et al. from the microwave spectrum [50–52], the value being  $r_{O \cdots O} = 2.98 \pm 0.04$  Å. Lane [53] has calculated a value of  $r_{O \cdots O} = 2.91$  Å (truncated value to the hundredth of Å) as the best estimation. The O–H distances depend on the role of the water molecules, with values of  $r_{OH} = 0.958$  pm Å and  $r_{OH} = 0.95$  Å when water is a donor or acceptor, respectively [48]. Bader et al. [45] have obtained that  $\rho_b$  and  $\nabla^2\rho_b$  are 0.0199 and 0.0624 (data in au), respectively. Other values can be found elsewhere [54,55]. From the four values of  $\rho_b$  (Table 1), an average value of 0.020 au is obtained, which matches the one for the water dimer. The  $\nabla^2\rho_b$  value for H–O–H  $\cdots$  OH<sub>2</sub> is closer to those in which the oxygens (O<sup>12</sup>) of hydroxy groups are donors and O<sup>w</sup> is an acceptor. It should be noticed that in these last two cases, the  $r_{OO}$  lengths are also closer to that of the H–O–H  $\cdots$  OH<sub>2</sub> dimer.

The mutual penetration of the hydrogen (H) and acceptor atoms (A, oxygen) is another criterion of hydrogen bond formation. This criterion is often considered a necessary and sufficient condition for the classification of an intermolecular interaction as hydrogen bonding [56]. It is estimated as  $\Delta r_i = r_i - r_i^o$  ( $i$ , are the atoms involved in the hydrogen bond, A or H),  $r_i$  being the bonded radius of each atom and  $r_i^o$  the corresponding nonbonded radius [44]. The nonbonded radius is the distance of a nucleus from a given electron density contour (usually 0.001 au) in the absence of interaction. This value is taken because it yields atomic diameters in good agreement with van der Waals radii in the gas phase [44]. The bonded radius is the distance from a nucleus to the bond critical point (HBCP). Numbers 17, 43, 50, and 59 identify these HBCPs in Figure 6. Table 1 shows the HBCP  $\cdots$  O and HBCP  $\cdots$  H lengths calculated for the complex. Obviously, the sum of both lengths should coincide with the imposed one from the crystal ( $r_1 + r_2 = r_{O \cdots H}$  length in Table 1). The HBCP  $\cdots$  H length,  $r_2$ , for the hydrogen bonds with O<sup>w</sup> as acceptor is larger (>0.1 Å) than those for O<sup>w</sup> being the donor. All of them are considerable smaller than this distance for the water dimer in the gas phase (=1.34 Å). Accepting that  $r_H^o = r_{vdW}^H = 1.1$  Å [57],  $\Delta r_H < 0$  in all cases. Similarly, if  $r_{vdW}^O = r_O^o = 1.58$  Å [57], then  $\Delta r_O < 0$ . These data provide evidence of a mutual penetration of hydrogen and oxygen atoms, a conclusion which may be raised from checking the contour electron density values of Figures 4 and 5. It should be noted that Isaev has defined [56]  $\Delta r_i = r_i^o - r_i$ , i.e.,  $\Delta r_O = r_{vdW}^O - r_{O \cdots HBCP}$  and  $\Delta r_H = r_{vdW}^H - r_{H \cdots HBCP}$ . In all cases,  $\Delta r_H > \Delta r_O$ , meaning that the hydrogen atom is more penetrated than the acceptor one.

## 2.2. Complexes O<sup>12a</sup>-H $\cdots$ O<sup>w</sup>-H $\cdots$ O<sup>7a</sup>, O<sup>12b</sup>-H $\cdots$ O<sup>w</sup>-H $\cdots$ O<sup>7b</sup> and O<sup>12a</sup>-H/H $\cdots$ O<sup>7a</sup>//O<sup>12b</sup>-H/H $\cdots$ O<sup>7b</sup>

Without changing the coordinates of the atoms, the whole complex O<sup>12a</sup>-H  $\cdots$  O<sup>w</sup>-H  $\cdots$  O<sup>7a</sup>//O<sup>12b</sup>-H  $\cdots$  O<sup>w</sup>-H  $\cdots$  O<sup>7b</sup> can be divided into two independent complexes, O<sup>12a</sup>-H  $\cdots$  O<sup>w</sup>-H  $\cdots$  O<sup>7a</sup> and O<sup>12b</sup>-H  $\cdots$  O<sup>w</sup>-H  $\cdots$  O<sup>7b</sup>, in which the water molecule only interacts with one of the pseudo-steroid residues of the original complex. It must be noticed that in both hemicomplexes, the water molecule is participating in the formation of two hydrogen bonds, being an acceptor and donor towards the O<sup>12</sup> and O<sup>7</sup> oxygen atoms, respectively. Thus, in each complex, only one O–H bond of water participates as a donor.

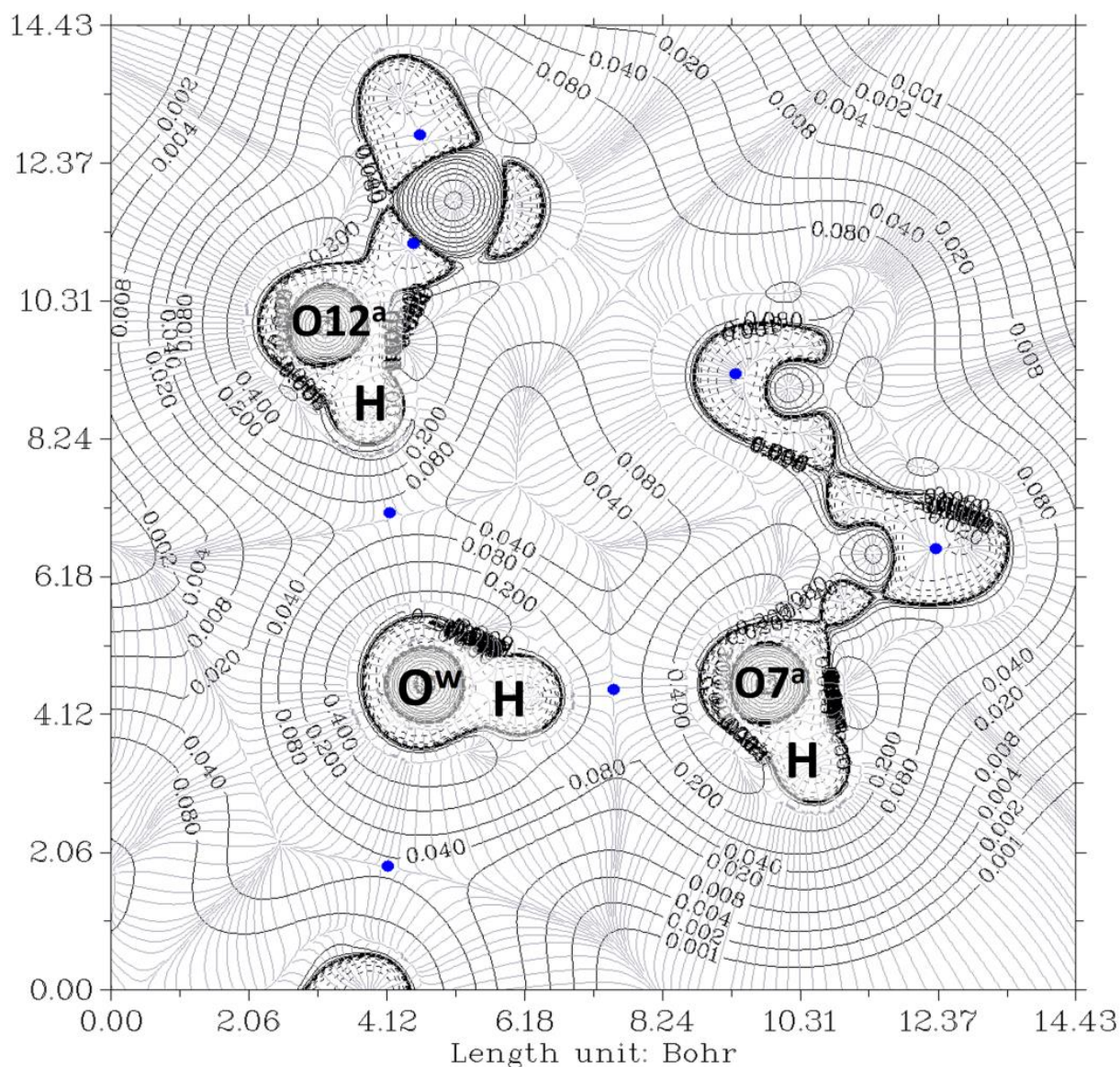


**Figure 6.** The electron density contour of the  $O^{12a}\text{-H}\cdots O^w\text{-H}\cdots O^{7a}$  complex (thin black lines) and BCP (3,-1) (blue dots).  $O^{12a}$ ,  $O^{7a}$ , and  $O^w$  are oxygen atoms from the pseudo-bile acid residues and water, respectively. Thin gray lines correspond to the gradient of the electron density.

Figures 6 and 7 show the contour lines at the planes defined by  $O^{7a}\text{-}O^w\text{-}O^{12a}$  and  $O^{7b}\text{-}O^w\text{-}O^{12b}$ , respectively. In both cases,  $O^w$  and  $O^{12}$  exhibit peanut profiles directed towards the associated acceptor atoms  $O^7$  and  $O^w$ , respectively. In all cases, the bond paths of the four hydrogen bonds link the expected two atoms, and the HBCP is indicated with a blue color point. The analysis of the data was carried out as previously. The HBCPs are identified by numbers (Figure not shown), and, for association purposes, the HBCPs of the full complex are shown in brackets. Table 2 shows the obtained results.

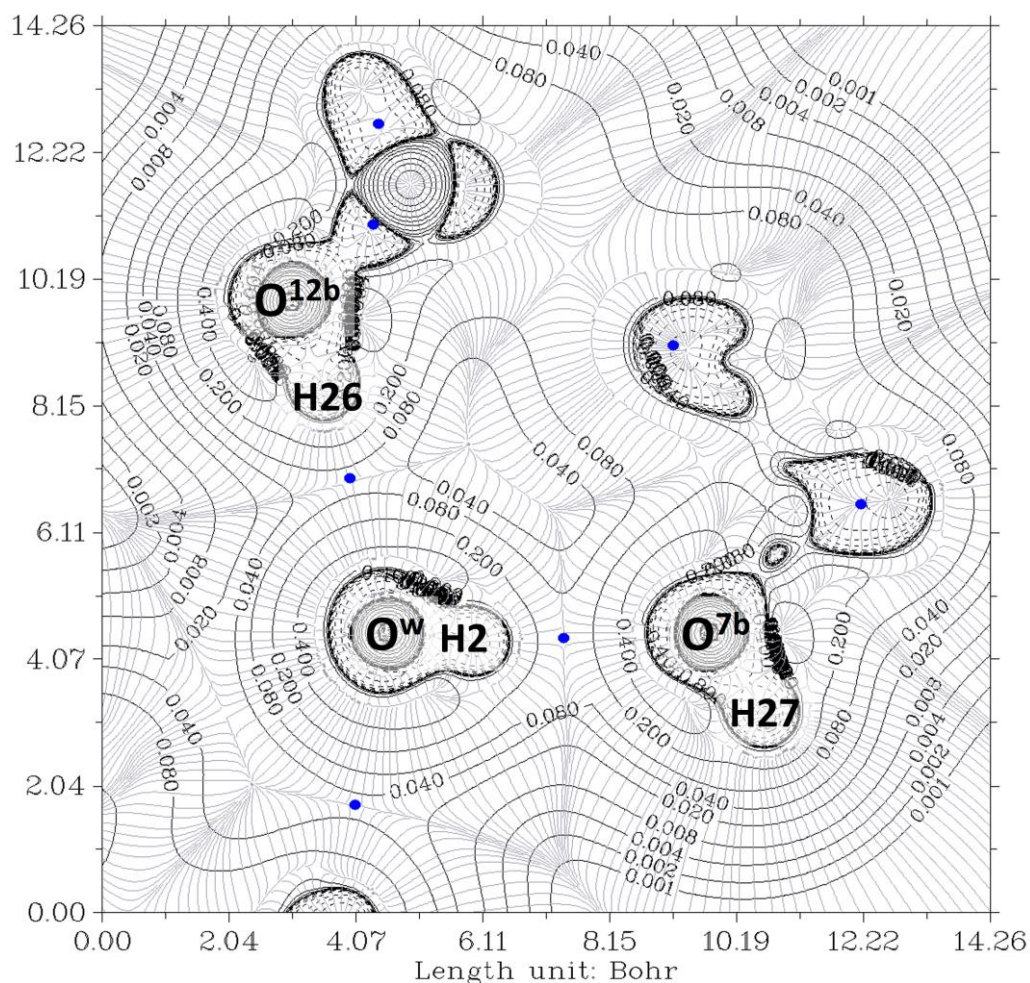


**Figure 7.** The electron density contour of the  $O^{7b}$ - $O^w$ - $O^{12b}$  complex (thin black lines) and BCP (3,-1) (blue dots).  $O^{12b}$ ,  $O^{7b}$ , and  $O^w$  are oxygen atoms from the pseudo-bile acid residues and water, respectively. Thin gray lines correspond to the gradient of the electron density.

**Table 2.** Electron density, Laplacian of the electron density, and lengths involved in the formation of hydrogen bonds of the two semi complexes:  $O^{12a}$ -H...  $O^w$ -H...  $O^{7a}$  and  $O^{12a}$ -H...  $O^w$ -H...  $O^{7a}$ .

Property at HBCP	$O^{12a}$ -H... $O^w$ -H... $O^{7a}$		$O^{12b}$ -H... $O^w$ -H... $O^{7b}$	
	CP71 (CP50) $O^{12a}$ -H... $O^w$	CP74 (CP59) $O^w$ -H... $O^{7a}$	CP68 (CP17) $O^{12b}$ -H... $O^w$	CP71 (CP43) $O^w$ -H... $O^{7b}$
Electron density $\rho_b$ , au	0.0152	0.0239	0.0137	0.0270
Laplacian of $\rho_b$ , $\nabla^2 \rho_b$ , au	0.0662	0.106	0.0610	0.119
HBCP ... O length/Å, $r_1$	1.353	1.243	1.381	1.218
HBCP ... H length/Å, $r_2$	0.761	0.679	0.797	0.650
$r_1 + r_2 = O \dots H$ length/Å	2.115	1.922	2.177	1.867

It may be observed that all the values in Table 2 perfectly match those in Table 1. This is partially due to the fact that the original geometric parameters of the C-H<sub>2</sub>O-C crystal are kept constant. Because of previous agreements, the mutual penetration of hydrogen and oxygen atoms is not discussed.

Finally, the electron density of the complex without water,  $O^{12a}$ -H/H...  $O^{7a}$ // $O^{12b}$ -H/H...  $O^{7b}$ , has also been studied. Figure 8 shows the contour map of the two halves of

the complex. As it was expected, the contour lines strongly differ from previous ones, and HBCP are not observed.

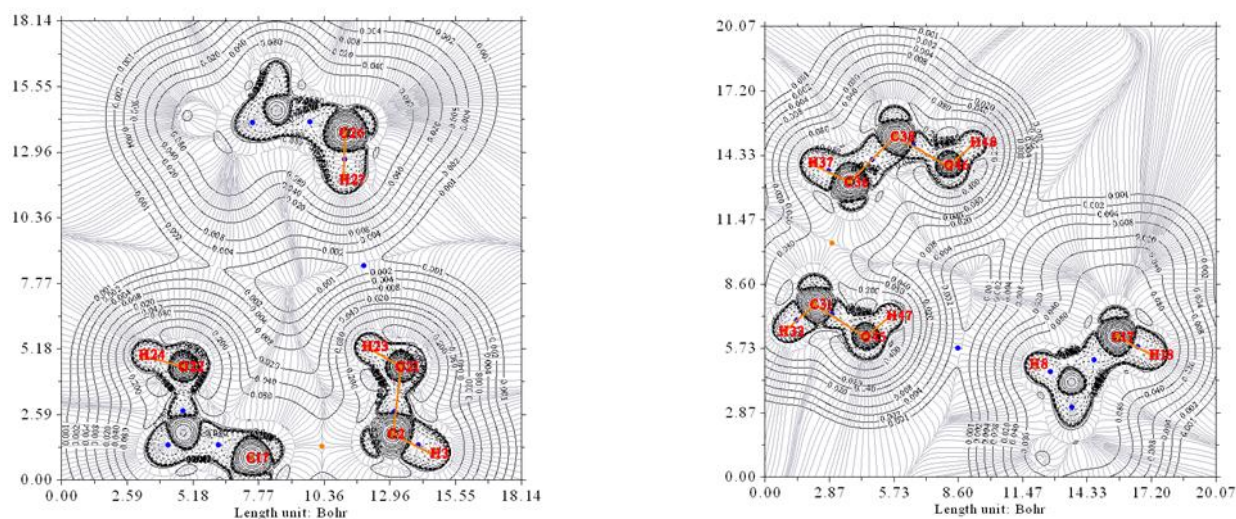


**Figure 8.** The electron density contour of the  $O^{12a}\text{-H/H}\cdots O^{7a}/O^{12b}\text{-H/H}\cdots O^{7b}$  complex (thin black lines).  $O^{7a}$  and  $O^{7b}$  are oxygen atoms from the pseudo-bile acid residues. Thin gray lines correspond to the gradient of the electron density.

### 2.3. Energy of Hydrogen Bonds

The interaction energy for the formation of the complex  $O^{12a}\text{-H}\cdots O^w\text{-H}\cdots O^{7a}/O^{12b}\text{-H}\cdots O^w\text{-H}\cdots O^{7b}$  is  $-54.29\text{ kJ mol}^{-1}$ . This value cannot be exclusively ascribed to the formation of the four hydrogen bonds. In fact, for the complex  $O^{12a}\text{-H/H}\cdots O^{7a}/O^{12b}\text{-H/H}\cdots O^{7b}$  (in which the water molecule has been removed), a value of  $-4.60\text{ kJ/mol}$  has been calculated. Because of the length differences between the hydrogen bonds in which  $O^w$  is the donor and those in which it is the acceptor ( $2.7\text{ \AA}$  vs.  $2.9\text{ \AA}$ ), the energy of each hydrogen bond is expected to be different [58]. Having these considerations in mind, the average energy of the hydrogen bonds is  $-13.57\text{ kJ/mol}$ . Such a value indicates that they are moderate hydrogen bonds according to Jeffrey's categories [59] or weak to medium according to the ranges proposed by Emamian et al. [60]. Rocher-Casterline et al. [61] have determined a value of  $13.2 \pm 0.5\text{ kJ mol}^{-1}$  for the bond dissociation energy ( $D_0$ ) of the water dimer. Ruscic [62], from a new partition function for water, has obtained dissociation enthalpy values for the water dimer, the values being  $13.220 \pm 0.096\text{ kJ mol}^{-1}$  and  $15.454 \pm 0.074\text{ kJ mol}^{-1}$  at  $0\text{ K}$  and  $298.15\text{ K}$ , respectively, and Feyereisen et al. [63], from the thermal conductivity of the vapor, measured a value of  $-15.07 \pm 2.1\text{ kJ mol}^{-1}$ . Most of the values calculated theoretically for this dimer are within the interval  $-13.4/-23.1\text{ kJ mol}^{-1}$  [45,53–55,60,63–66].

For the formation of hydrogen bonds between water and methanol, in gas phase, Moin et al. [67] have obtained values of  $1.96\text{--}2.04\text{ \AA}$  ( $O_{\text{meth}}\text{H}\cdots O_w$ ) and  $1.94\text{--}2.02\text{ \AA}$  ( $O_w\text{H}\cdots O_{\text{meth}}$ ), for the  $\text{H}\cdots\text{O}$  distances, while the hydrogen bond energies were in the ranges of  $-20.45/-27.04\text{ kJ mol}^{-1}$  ( $O_{\text{meth}}\text{H}\cdots O_w$ ) and  $-21.24/-29.39\text{ kJ mol}^{-1}$  ( $O_w\text{H}\cdots O_{\text{meth}}$ ), the values depending on the level of the theory. These values are in line with the different behavior of water depending on whether it is a donor or acceptor, as observed previously.

For a series of hydrogen-bonded complexes between nitrites and hydrogen chloride, Boyd and Choi [68] have noticed a correlation between the electron density at the HBCP  $\rho_b$  and the energy of the hydrogen bond. The energies ranged from  $10\text{ kJ/mol}$  to  $38\text{ kJ/mol}$ , while the range of  $\rho_b$  was  $0.01103\text{--}0.02391$ . Many other equations have been published; the subject is being reviewed by Rozenberg [69]. There is no objective reason to choose one

or another equation for the present system, and as an orientation, we will use the following relationship that Rozenberg obtained from 24 equations:

$$E(\text{kJ/mol}) = -(6.6 \pm 8.0) + (1215 \pm 440)\rho$$

After its application to each hydrogen bond of the present system, the summation of the individual values gives a total energy of  $-72 \pm 24$  kJ/mol, with a high standard deviation.

As indicated above, the nature of the complex  $\text{O}^{12a}\text{-H}/\text{H} \cdots \text{O}^{7a} // \text{O}^{12b}\text{-H}/\text{H} \cdots \text{O}^{7b}$  allows the calculation of the interaction of two subsystems,  $\text{O}^{12a}\text{-H} \cdots \text{O}^{\text{w-H}} \cdots \text{O}^{7a}$  and  $\text{O}^{12b}\text{-H} \cdots \text{O}^{\text{w-H}} \cdots \text{O}^{7b}$ , both having two hydrogen bonds with water acting as donor and acceptor. The calculated values are  $-25.91$  kJ/mol and  $-21.18$  kJ/mol for the “a” and “b” subsystems, respectively. By considering the interaction energy between the two pseudosteroids (see above) and the previous values, the difference between the calculated energy of the whole system and that resulting from the sum of the three subsystems is only 2.5 kJ/mol.

### 3. Materials and Methods

#### *Crystal Structure and Computational Details*

The crystal structure of the reference system (C-H<sub>2</sub>O-C) was previously published [8]. In this reference, a complete image of Figure 2, is shown on the left. The Cif files (CCDC 867499) contain the supplementary crystallographic data for the C-succ-C crystal (the acronym given in that paper). These data can be obtained free of charge from the Cambridge Crystallographic Data Center via [www.ccdc.cam.ac.uk/data\\_request/cif](http://www.ccdc.cam.ac.uk/data_request/cif).

Given the high number of atoms involved in the two bile acid dimers, to analyze the interaction with the water molecule, we have simplified the system by reducing the number of atoms in the bile acid unit while keeping the same geometric parameters of the remaining atoms. Thus, A and D rings were suppressed, and the carbon atoms linking them to B and C rings were replaced by hydrogen atoms. This system will be referred to as  $\text{O}^{12a}\text{-H} \cdots \text{O}^{\text{w-H}} \cdots \text{O}^{7a} // \text{O}^{12b}\text{-H} \cdots \text{O}^{\text{w-H}} \cdots \text{O}^{7b}$ , where the superscripts “a” and “b” refer to the upper and lower pseudo-bile acid residues, respectively (see Figure 2). This complex is later divided into two independent subsystems, named  $\text{O}^{12a}\text{-H} \cdots \text{O}^{\text{w-H}} \cdots \text{O}^{7a}$  and  $\text{O}^{12b}\text{-H} \cdots \text{O}^{\text{w-H}}$ , which allow the calculation of the interaction of the water molecule with only one of the pseudo-steroid residues. The interaction between the two pseudo-bile acid residues, without water complexed between them,  $\text{O}^{12a}\text{-H}/\text{H} \cdots \text{O}^{7a} // \text{O}^{12b}\text{-H}/\text{H} \cdots \text{O}^{7b}$ , has also been studied.

We have maintained the original interatomic distances obtained from the x-ray resolution of the C-H<sub>2</sub>O-C complex, and no minimization of the energy of the complex was carried out. Calculations of the complexation energy used for correction of the basis set superposition error (BSSE) with the counterpoise method implemented in Gaussian 19 [70]. Laplacian of electronic density and critical points (AIM) were calculated using the Multiwfn\_3.8\_dev software [71].

### 4. Conclusions

There are two main oxygen-oxygen ( $r_{\text{OO}}$ ) distances when a hydrogen bond is formed between water molecules: the one observed in the gas phase in the formation of a dimer ( $r_{\text{OO}} = 2.98$  Å) and the one in ice ( $r_{\text{OO}} = 2.75$  Å). Both lengths are observed in the C-succ-C crystal, in which a water molecule is encapsulated by four hydroxy groups belonging to two cholic acid dimers. The shorter one corresponds to hydrogen bonds in which the water oxygen is donor and the larger one when it is the acceptor. The application of the AIM theory to a simplified system  $\text{O}^{12a}\text{-H} \cdots \text{O}^{\text{w-H}} \cdots \text{O}^{7a} // \text{O}^{12b}\text{-H} \cdots \text{O}^{\text{w-H}} \cdots \text{O}^{7b}$  confirms the existence of saddle critical points (HBCP) in all four of these hydrogen bonds. The estimated interaction energy in the formation of the complex,  $-54.29$  kJ mol<sup>-1</sup>, is in acceptable agreement with the summation of the energies of the two hemicomplexes,  $\text{O}^{12a}\text{-H} \cdots \text{O}^{\text{w-H}} \cdots \text{O}^{7a}$  and  $\text{O}^{12b}\text{-H} \cdots \text{O}^{\text{w-H}} \cdots \text{O}^{7b}$ , in which the water molecule forms two hydrogen bonds (acting as donor and acceptor) and the interaction energy of the

two pseudo-steroid nucleus  $O^{12a}\text{-H/H}\cdots O^{7a}/O^{12b}\text{-H/H}\cdots O^{7b}$  (i.e., without complexed water). This fact and the calculated values for the electron density, the Laplacian of the electron density, and the lengths of the oxygen atom and the hydrogen atom (involved in the formation of each hydrogen bond) to the HBCP suggest that each pair of hydrogen bonds can be considered independent of each other.

**Author Contributions:** Conceptualization, J.A.S. and J.V.T.; methodology, J.A.S. and J.V.T.; formal analysis, M.P.V.-T., F.M., J.A.S. and J.V.T.; investigation, M.P.V.-T., F.M. and S.d.F.; writing—original draft preparation, writing—review and editing, M.P.V.-T., F.M., J.A.S. and J.V.T.; funding acquisition, M.P.V.-T., F.M., J.A.S. and J.V.T. All authors have read and agreed to the published version of the manuscript.

**Funding:** This work was funded by the Ministerio de Ciencia y Tecnología, Spain (Project MAT201786109P).

**Acknowledgments:** Part of this paper was presented at the 26th International Electronic Conference on Synthetic Organic Chemistry. 15–30 November 2022.

**Conflicts of Interest:** The authors declare no conflict of interest.

## References

1. Menger, F.M. Supramolecular chemistry and self-assembly. *Proc. Natl. Acad. Sci. USA* **2002**, *99*, 4818–4822. [[CrossRef](#)] [[PubMed](#)]
2. Lehn, J.-M. Toward complex matter: Supramolecular chemistry and self-organization. *Proc. Natl. Acad. Sci. USA* **2002**, *99*, 4763–4768. [[CrossRef](#)]
3. Hofmann, A.F.; Hagey, L.R.; Krasowski, M.D. Bile salts of vertebrates: Structural variation and possible evolutionary significance. *J. Lipid Res.* **2010**, *51*, 226–246. [[CrossRef](#)]
4. Soto, V.H.; Jover, A.; Meijide, F.; Vázquez Tato, J.; Galantini, L.; Pavel, N.V. Supramolecular structures generated by a p-tert-butylphenyl-amide derivative of cholic acid. From vesicles to molecular tubes. *Adv. Mater.* **2007**, *19*, 1752–1756. [[CrossRef](#)]
5. Miragaya, J.; Jover, A.; Fraga, F.; Meijide, F.; Tato, J.V. Enantioresolution and Chameleonic Mimicry of 2-Butanol with an Adamantylacetyl Derivative of Cholic Acid. *Cryst. Growth Des.* **2010**, *10*, 1124–1129. [[CrossRef](#)]
6. Manghisi, N.; Leggio, C.; Jover, A.; Meijide, F.; Pavel, N.V.; Tellini, V.H.S.; Tato, J.V.; Agostino, R.G.; Galantini, L. Catanionic Tubules with Tunable Charge. *Angew. Chem. Int. Ed.* **2010**, *49*, 6604–6607. [[CrossRef](#)]
7. Galantini, L.; di Gregorio, M.C.; Gubitosi, M.; Travaglini, L.; Vázquez Tato, J.; Jover, A.; Meijide, F.; Tellini, V.H.S.; Pavel, N.V. Bile salts and derivatives: Rigid un-conventional amphiphiles as dispersants, carriers and superstructure building blocks. *Curr. Opin. Colloid Interface Sci.* **2015**, *20*, 170–182. [[CrossRef](#)]
8. Soto, V.H.; Alvarez, M.; Meijide, F.; Trillo, J.V.; Antelo, A.; Jover, A.; Galantini, L.; Tato, J.V. Ice-like encapsulated water by two cholic acid moieties. *Steroids* **2012**, *77*, 1228–1232. [[CrossRef](#)] [[PubMed](#)]
9. Meijide, F.; de Frutos, S.; Soto, V.H.; Jover, A.; Seijas, J.A.; Vázquez-Tato, M.P.; Fraga, F.; Tato, J.V. A Standard Structure for Bile Acids and Derivatives. *Crystals* **2018**, *8*, 86. [[CrossRef](#)]
10. Giglio, E. Structural aspect of inclusion compounds formed by organic host lattices. In *Inclusion Compounds of Deoxycholic Acid*; Atwood, J.L., Davies, J.E.D., MacNicol, D.D., Eds.; Academic Press: London, UK, 1984; pp. 207–229.
11. Miyata, M.; Sada, K. Deoxycholic acid and related hosts. In *Comprehensive Supra-Molecular Chemistry 6*; MacNicol, D.D.T.F., Bishop, R., Eds.; Elsevier: Oxford, UK, 1996; pp. 147–176.
12. Campanelli, A.R.; De Sanctis, S.C.; Giglio, E.; Pavel, N.V.; Quagliata, C. From crystal to micelle: A new approach to the micellar structure. *J. Incl. Phenom. Macrocycl. Chem.* **1989**, *7*, 391–400. [[CrossRef](#)]
13. Sada, K.; Sugahara, M.; Kato, K.; Miyata, M. Controlled Expansion of a Molecular Cavity in a Steroid Host Compound. *J. Am. Chem. Soc.* **2001**, *123*, 4386–4392. [[CrossRef](#)] [[PubMed](#)]
14. Sugahara, M.; Sada, K.; Miyata, M. A robust structural motif in inclusion crystals of nor-bile acids. *Chem. Commun.* **1999**, *3*, 293–294. [[CrossRef](#)]
15. Sugahara, M.; Hirose, J.; Sada, K.; Miyata, M. Inclusion Abilities of Bile Acids with Different Side Chain Length. *Mol. Cryst. Liq. Cryst.* **2001**, *356*, 155–162. [[CrossRef](#)]
16. Hishikawa, Y.; Aoki, Y.; Sada, K.; Miyata, M. Selective Inclusion Phenomena in Lithocholamide Crystal Lattices; Design of Bilayered Assemblies through Ladder-type Hydrogen Bonding Network. *Chem. Lett.* **1998**, *27*, 1289–1290. [[CrossRef](#)]
17. Miyata, M.; Tohnai, N.; Hisaki, I. Supramolecular Chirality in Crystalline Assemblies of Bile Acids and Their Derivatives; Three-Axial, Tilt, Helical, and Bundle Chirality. *Molecules* **2007**, *12*, 1973–2000. [[CrossRef](#)]
18. Fletcher, N.H. *The Chemical Physics of Ice. The Chemical Physics of Ice*; Cambridge University Press: Cambridge, UK, 1970.
19. Bergmann, U.; Di Cicco, A.; Wernet, P.; Principi, E.; Glatzel, P.; Nilsson, A. Nearest-neighbor oxygen distances in liquid water and ice observed by x-ray Raman based extended x-ray absorption fine structure. *J. Chem. Phys.* **2007**, *127*, 174504. [[CrossRef](#)]
20. Steiner, T. The Hydrogen Bond in the Solid State. *Angew. Chem. Int. Ed.* **2002**, *41*, 48–76. [[CrossRef](#)]
21. Atwood, J.L.; Barbour, L.J.; Ness, T.J.; Raston, C.L.; Raston, P.L. A Well-Resolved Ice-like (H<sub>2</sub>O)<sub>8</sub> Cluster in an Organic Supramolecular Complex. *J. Am. Chem. Soc.* **2001**, *123*, 7192–7193. [[CrossRef](#)]

22. Barbour, L.J.; Orr, G.W.; Atwood, J.L. An intermolecular (H<sub>2</sub>O)<sub>10</sub> cluster in a solid-state supramolecular complex. *Nature* **1998**, *393*, 671–673. [[CrossRef](#)]
23. Barbour, L.; Orr, G.; Atwood, J. CCDC 145404: Experimental Crystal Structure Determination. *Chem. Commun.* **2000**, 859. [[CrossRef](#)]
24. Hoelzl, C.; Horinek, D. Pressure increases the ice-like order of water at hydrophobic interfaces. *Phys. Chem. Chem. Phys.* **2018**, *20*, 21257–21261. [[CrossRef](#)]
25. Saha, B.K.; Nangia, A. First example of an ice-like water hexamer boat tape structure in a supramolecular organic host. *Chem. Commun.* **2006**, *12*, 1825–1827. [[CrossRef](#)]
26. Smolin, N.; Daggett, V. Formation of Ice-like Water Structure on the Surface of an Antifreeze Protein. *J. Phys. Chem. B* **2008**, *112*, 6193–6202. [[CrossRef](#)] [[PubMed](#)]
27. Mahatabuddin, S.; Fukami, D.; Arai, T.; Nishimiya, Y.; Shimizu, R.; Shibasaki, C.; Kondo, H.; Adachi, M.; Tsuda, S. Polypentagonal ice-like water networks emerge solely in an activity-improved variant of ice-binding protein. *Proc. Natl. Acad. Sci. USA* **2018**, *115*, 5456–5461. [[CrossRef](#)] [[PubMed](#)]
28. Odendahl, N.L.; Geissler, P.L. Local Ice-like Structure at the Liquid Water Surface. *J. Am. Chem. Soc.* **2022**, *144*, 11178–11188. [[CrossRef](#)] [[PubMed](#)]
29. Bonn, M.; Bakker, H.J.; Tong, Y.; Backus, E.H.G. No Ice-Like Water at Aqueous Biological Interfaces. *Biointerphases* **2012**, *7*, 20. [[CrossRef](#)]
30. He, Z.; Zhou, J.; Lu, X.; Corry, B. Ice-like Water Structure in Carbon Nanotube (8,8) Induces Cationic Hydration Enhancement. *J. Phys. Chem. C* **2013**, *117*, 11412–11420. [[CrossRef](#)]
31. Takaiwa, D.; Hatano, I.; Koga, K.; Tanaka, H. Phase diagram of water in carbon nanotubes. *Proc. Natl. Acad. Sci. USA* **2008**, *105*, 39–43. [[CrossRef](#)]
32. Pascal, T.A.; Goddard, W.A.; Jung, Y. Entropy and the driving force for the filling of carbon nanotubes with water. *Proc. Natl. Acad. Sci. USA* **2011**, *108*, 11794–11798. [[CrossRef](#)]
33. Agrawal, K.V.; Shimizu, S.; Drahusuk, L.W.; Kilcoyne, D.; Strano, M.S. Observation of extreme phase transition temperatures of water confined inside isolated carbon nanotubes. *Nat. Nanotechnol.* **2017**, *12*, 267–273. [[CrossRef](#)]
34. Sugiyama, Y.; Futamura, R.; Iiyama, T. Ice-like Structure of Water Confined in Hydrophobic Sub-nanometer Spaces at Room Temperature. *Chem. Lett.* **2022**, *51*, 760–764. [[CrossRef](#)]
35. Banerjee, D.; Bhat, S.N.; Bhat, S.V.; Leporini, D. Molecular probe dynamics reveals suppression of ice-like regions in strongly confined supercooled water. *PLoS ONE* **2012**, *7*, e44382. [[CrossRef](#)] [[PubMed](#)]
36. Weissmann, M.; Blum, L.; Cohan, N.V. On the hydrogen bond in an ice-like structure. *Chem. Phys. Lett.* **1967**, *1*, 95–98. [[CrossRef](#)]
37. Sun, D.; Xu, H.-R.; Yang, C.-F.; Wei, Z.-H.; Zhang, N.; Huang, R.-B.; Zheng, L.-S. Encapsulated Diverse Water Aggregates in Two Ag(I)/4,4'-Bipyridine/Dicarboxylate Hosts: 1D Water Tape and Chain. *Crystal Growth Des.* **2010**, *10*, 4642–4649. [[CrossRef](#)]
38. Ma, B.-Q.; Sun, H.-L.; Gao, S. Cyclic water pentamer in a tape-like structure. *Chem. Commun.* **2004**, *19*, 2220–2221. [[CrossRef](#)]
39. Popelier, P.L.A. On the full topology of the Laplacian of the electron density On the full topology of the Laplacian of the electron density. *Coord. Chem Rev.* **2000**, *197*, 169–189. [[CrossRef](#)]
40. Bader, R.F.W. Atoms in Molecules. *Acc. Chem. Res.* **1985**, *18*, 9–15. [[CrossRef](#)]
41. Grabowski, S.J. Hydrogen Bond—Definitions, Criteria of Existence and Various Types. In *Understanding Hydrogen Bonds: Theoretical and Experimental Views*; From Book Series: Theoretical and Computational Chemistry Series; Royal Society of Chemistry: London, UK, 2020; Chapter 1; pp. 1–40. [[CrossRef](#)]
42. Popelier, P.L.A. Characterization of a Dihydrogen Bond on the Basis of the Electron Density. *J. Phys. Chem. A* **1998**, *102*, 1873–1878. [[CrossRef](#)]
43. Carroll, M.T.; Chang, C.; Bader, R.F. Prediction of the structures of hydrogen-bonded complexes using the laplacian of the charge density. *Mol. Phys.* **1988**, *63*, 387–405. [[CrossRef](#)]
44. Koch, U.; Popelier, P.L.A. Characterization of C-H-O Hydrogen Bonds on the Basis of the Charge Density. *J. Phys. Chem.* **1995**, *99*, 9747–9754. [[CrossRef](#)]
45. Bader, R.F.W.; Carroll, M.T.; Cheeseman, J.R.; Chang, C. Properties of atoms in molecules: Atomic volumes. *J. Am. Chem. Soc.* **1987**, *109*, 7968–7979. [[CrossRef](#)]
46. Alkorta, I.; Rozas, I.; Elguero, J. Bond Length–Electron Density Relationships: From Covalent Bonds to Hydrogen Bond Interactions. *Struct. Chem.* **1998**, *9*, 243–247. [[CrossRef](#)]
47. Tang, T.-H.; Deretey, E.; Jensen, S.J.K.; Csizmadia, I.G. Hydrogen bonds: Relation between lengths and electron densities at bond critical points. *Eur. Phys. J. D* **2005**, *37*, 217–222. [[CrossRef](#)]
48. Mukhopadhyay, A.; Cole, W.T.; Saykally, R.J. The water dimer I: Experimental characterization. *Chem. Phys. Lett.* **2015**, *633*, 13–26. [[CrossRef](#)]
49. Mukhopadhyay, A.; Xantheas, S.S.; Saykally, R.J. The water dimer II: Theoretical investigations. *Chem. Phys. Lett.* **2018**, *700*, 163–175. [[CrossRef](#)]
50. Dyke, T.R.; Muentner, J.S. Microwave spectrum and structure of hydrogen bonded water dimer. *J. Chem. Phys.* **1974**, *60*, 2929–2930. [[CrossRef](#)]
51. Dyke, T.R.; Mack, K.M.; Muentner, J.S. The structure of water dimer from molecular beam electric resonance spectroscopy. *J. Chem. Phys.* **1977**, *66*, 498–510. [[CrossRef](#)]

52. Odutola, J.A.; Dyke, T.R. Partially deuterated water dimers: Microwave spectra and structure. *J. Chem. Phys.* **1980**, *72*, 5062–5070. [[CrossRef](#)]
53. Lane, J.R. CCSDTQ Optimized Geometry of Water Dimer. *J. Chem. Theory Comput.* **2013**, *9*, 316–323. [[CrossRef](#)]
54. Grabowski, S.J. Ab Initio Calculations on Conventional and Unconventional Hydrogen Bonds Study of the Hydrogen Bond Strength. *J. Phys. Chem. A* **2001**, *105*, 10739–10746. [[CrossRef](#)]
55. Kumar, P.S.V.; Raghavendra, V.; Subramanian, V. Bader's Theory of Atoms in Molecules (AIM) and its Applications to Chemical Bonding. *J. Chem. Sci.* **2016**, *128*, 1527–1536. [[CrossRef](#)]
56. Isaev, A.N. Ammonia and phosphine complexes with proton donors. Hydrogen bonding from the backside of the N(P) lone pair. *Comput. Theor. Chem.* **2018**, *1142*, 28–38. [[CrossRef](#)]
57. Rowland, R.S.; Taylor, R. Intermolecular Nonbonded Contact Distances in Organic Crystal Structures: Comparison with Distances Expected from van der Waals Radii. *J. Phys. Chem.* **1996**, *100*, 7384–7391. [[CrossRef](#)]
58. Wendler, K.; Thar, J.; Zahn, S.; Kirchner, B. Estimating the Hydrogen Bond Energy. *J. Phys. Chem. A* **2010**, *114*, 9529–9536. [[CrossRef](#)]
59. Jeffrey, G.J. *An Introduction to Hydrogen Bonding*; Oxford University Press: New York, NY, USA, 1997; p. 12.
60. Emamian, S.; Lu, T.; Kruse, H.; Emamian, H. Exploring Nature and Predicting Strength of Hydrogen Bonds: A Correlation Analysis Between Atoms-in-Molecules Descriptors, Binding Energies, and Energy Components of Symmetry-Adapted Perturbation Theory. *J. Comput. Chem.* **2019**, *40*, 2868–2881. [[CrossRef](#)]
61. Rocher-Casterline, B.E.; Ch'Ng, L.C.; Mollner, A.K.; Reisler, H. Communication: Determination of the bond dissociation energy ( $D_0$ ) of the water dimer,  $(\text{H}_2\text{O})_2$ , by velocity map imaging. *J. Chem. Phys.* **2011**, *134*, 211101. [[CrossRef](#)]
62. Ruscic, B. Active Thermochemical Tables: Water and Water Dimer. *J. Phys. Chem. A* **2013**, *117*, 11940–11953. [[CrossRef](#)]
63. Feyereisen, M.W.; Feller, D.; Dixon, D.A. Hydrogen Bond Energy of the Water Dimer. *J. Phys. Chem.* **1996**, *100*, 2993–2997. [[CrossRef](#)]
64. Grabowski, S.J. High-Level Ab Initio Calculations of Dihydrogen-Bonded Complexes. *J. Phys. Chem. A* **2000**, *104*, 5551–5557. [[CrossRef](#)]
65. Gu, Y.; Kar, T.; Scheiner, S. Fundamental Properties of the  $\text{CH}\cdots\text{O}$  Interaction: Is It a True Hydrogen Bond? *J. Am. Chem. Soc.* **1999**, *121*, 9411–9422. [[CrossRef](#)]
66. Shank, A.; Wang, Y.; Kaledin, A.; Braams, B.J.; Bowman, J.M. Accurate ab initio and “hybrid” potential energy surfaces, intramolecular vibrational energies, and classical ir spectrum of the water dimer. *J. Chem. Phys.* **2009**, *130*, 144314. [[CrossRef](#)] [[PubMed](#)]
67. Moin, S.T.; Hofer, T.S.; Randolf, B.R.; Rode, B.M. Structure and dynamics of methanol in water: A quantum mechanical charge field molecular dynamics study. *J. Comput. Chem.* **2011**, *32*, 886–892. [[CrossRef](#)] [[PubMed](#)]
68. Boyd, R.; Choi, S.C. Hydrogen bonding between nitriles and hydrogen halides and the topological properties of molecular charge distributions. *Chem. Phys. Lett.* **1986**, *129*, 62–65. [[CrossRef](#)]
69. Rozenberg, M. The hydrogen bond—Practice and QTAIM theory. *RSC Adv.* **2014**, *4*, 26928–26931. [[CrossRef](#)]
70. Frisch, M.J.; Trucks, G.W.; Schlegel, H.B.; Scuseria, G.E.; Robb, M.A.; Cheeseman, J.R.; Scalmani, G.; Barone, V.; Petersson, G.A.; Nakatsuji, H.; et al. *Gaussian 16 RC*; Gaussian, Inc.: Wallingford, CT, USA, 2016.
71. Lu, T.; Chen, F. Multiwfn: A multifunctional wavefunction analyzer. *J. Comput. Chem.* **2012**, *33*, 580–592. [[CrossRef](#)]

**Disclaimer/Publisher's Note:** The statements, opinions and data contained in all publications are solely those of the individual author(s) and contributor(s) and not of MDPI and/or the editor(s). MDPI and/or the editor(s) disclaim responsibility for any injury to people or property resulting from any ideas, methods, instructions or products referred to in the content.